An Overlapping Kinase and Phosphatase Docking Site Regulates Activity of the Retinoblastoma Protein

Alexander Hirschi, Matthew Cecchini, Rachel C. Steinhardt, Frederick A. Dick, and Seth M. Rubin

Supplementary Figures and Information

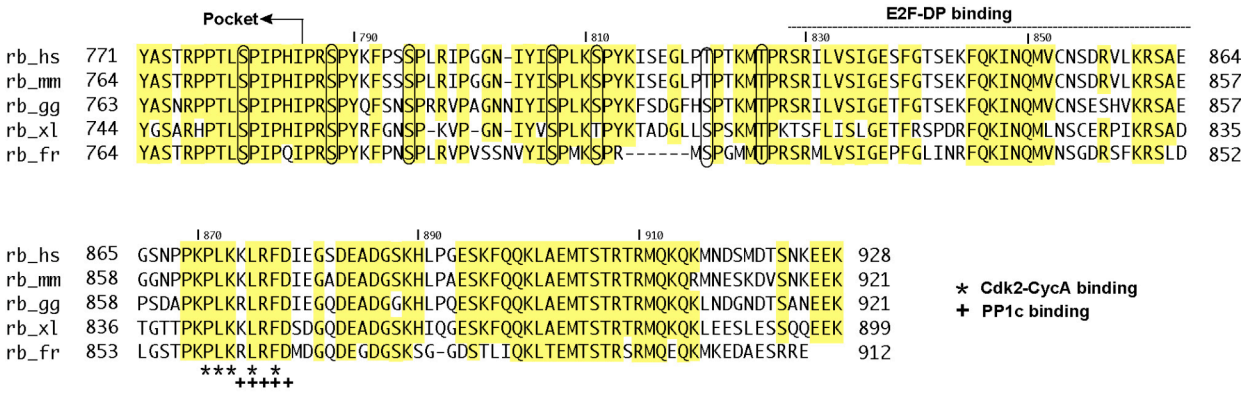

Supplementary Figure 1 Sequence alignment of RbC orthologs from human (hs), mouse (mm), chicken (gg), frog (xl), and fugu (fr). Numbering corresponds to the human sequence. Conservation is shown in yellow and Cdk consensus sites are circled. The E2F-DP binding sequence is indicated as well as the amino acids that contact CycA (*)[31] and PP1c (+).

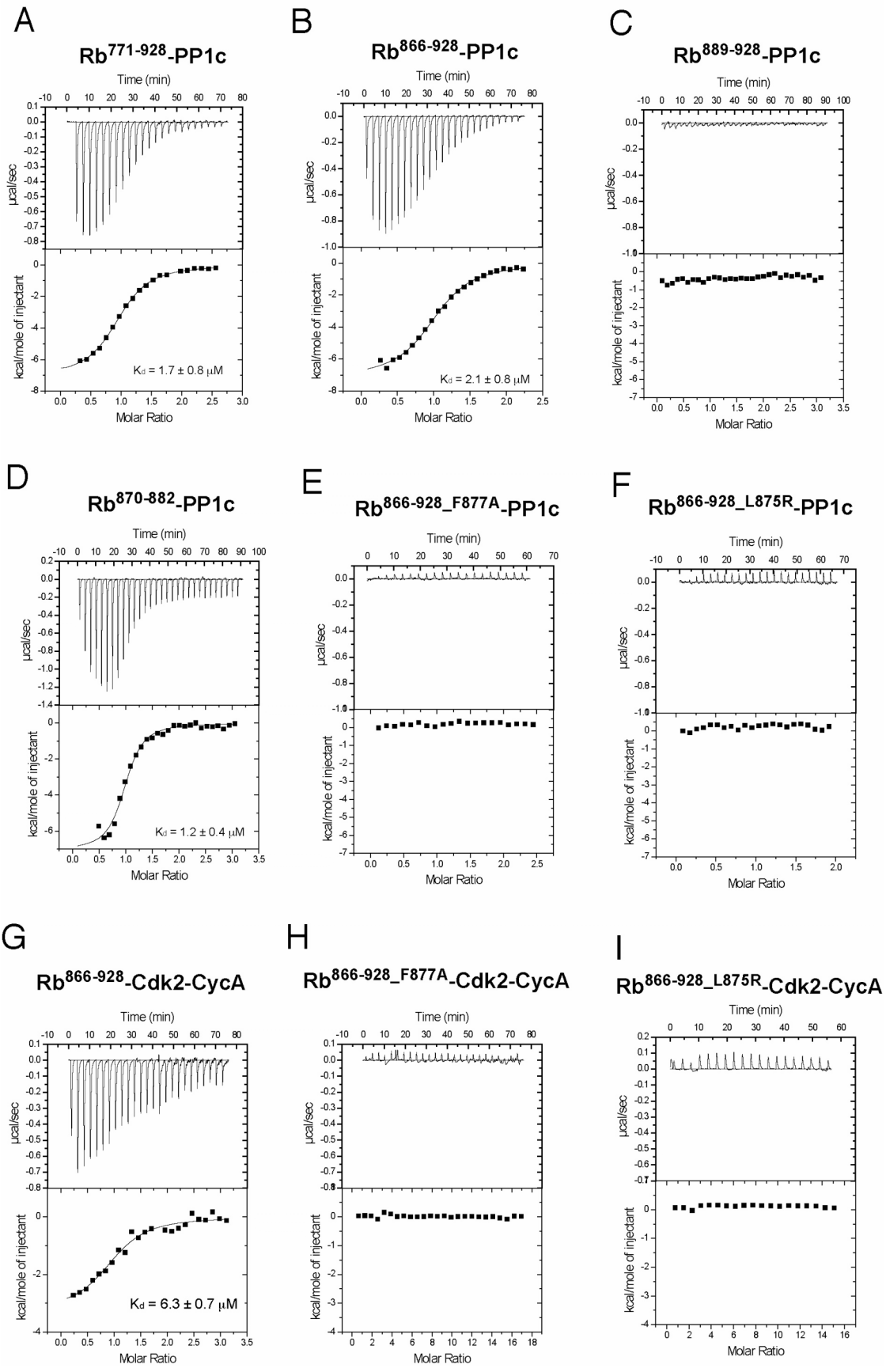
A
Rb771-928-PP1c
Time (min)
µcal/sec
kcal/mole of injectant
Kd = 1.7 ± 0.8 µM
Molar Ratio
B
Rb866-928-PP1c
Time (min)
µcal/sec
kcal/mole of injectant
Kd = 2.1 ± 0.8 µM
Molar Ratio
C
Rb889-928-PP1c
Time (min)
µcal/sec
kcal/mole of injectant
Molar Ratio
D
Rb870-882-PP1c
Time (min)
µcal/sec
kcal/mole of injectant
Kd = 1.2 ± 0.4 µM
Molar Ratio
E
Rb866-928_F877A-PP1c
Time (min)
µcal/sec
kcal/mole of injectant
Molar Ratio
F
Rb866-928_L875R-PP1c
Time (min)
µcal/sec
kcal/mole of injectant
Molar Ratio
G
Rb866-928-Cdk2-CycA
Time (min)
µcal/sec
kcal/mole of injectant
Kd = 6.3 ± 0.7 µM
Molar Ratio
H
Rb866-928_F877A-Cdk2-CycA
Time (min)
µcal/sec
kcal/mole of injectant
Molar Ratio
I
Rb866-928_L875R-Cdk2-CycA
Time (min)
µcal/sec
kcal/mole of injectant
Molar Ratio

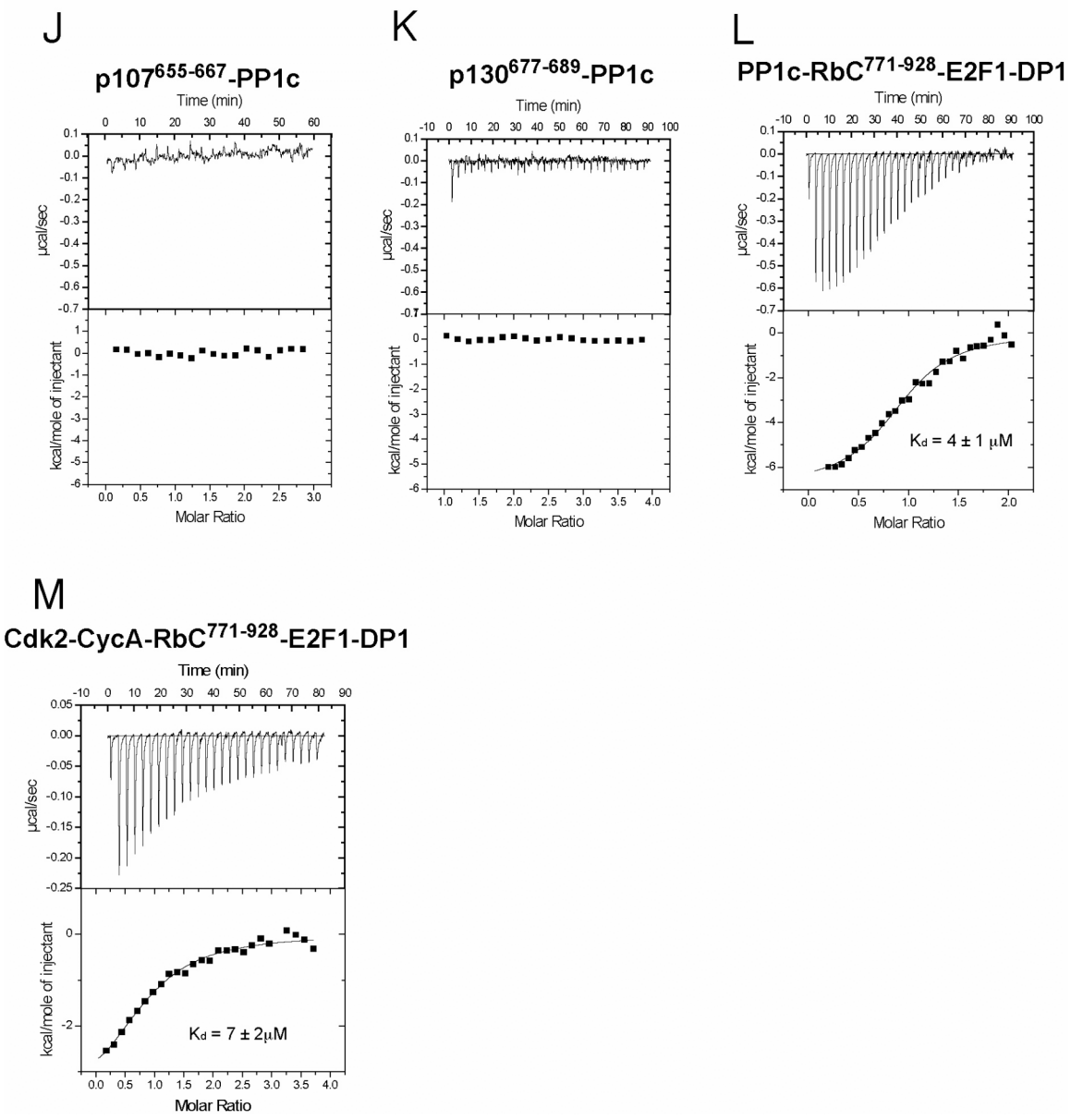

Supplementary Figure 2 Sample isothermal titration calorimetry data for binding assays. Raw data and isotherms are for binding reactions as indicated. Typically ~1 mM of the indicated RbC, P107, or P130 construct was titrated into a solution containing ~50 µM of PP1c or Cdk2-CycA. In (L) and (M), PP1c and Cdk-CycA were titrated into a solution containing preformed RbC-E1F1-DP1 complex.

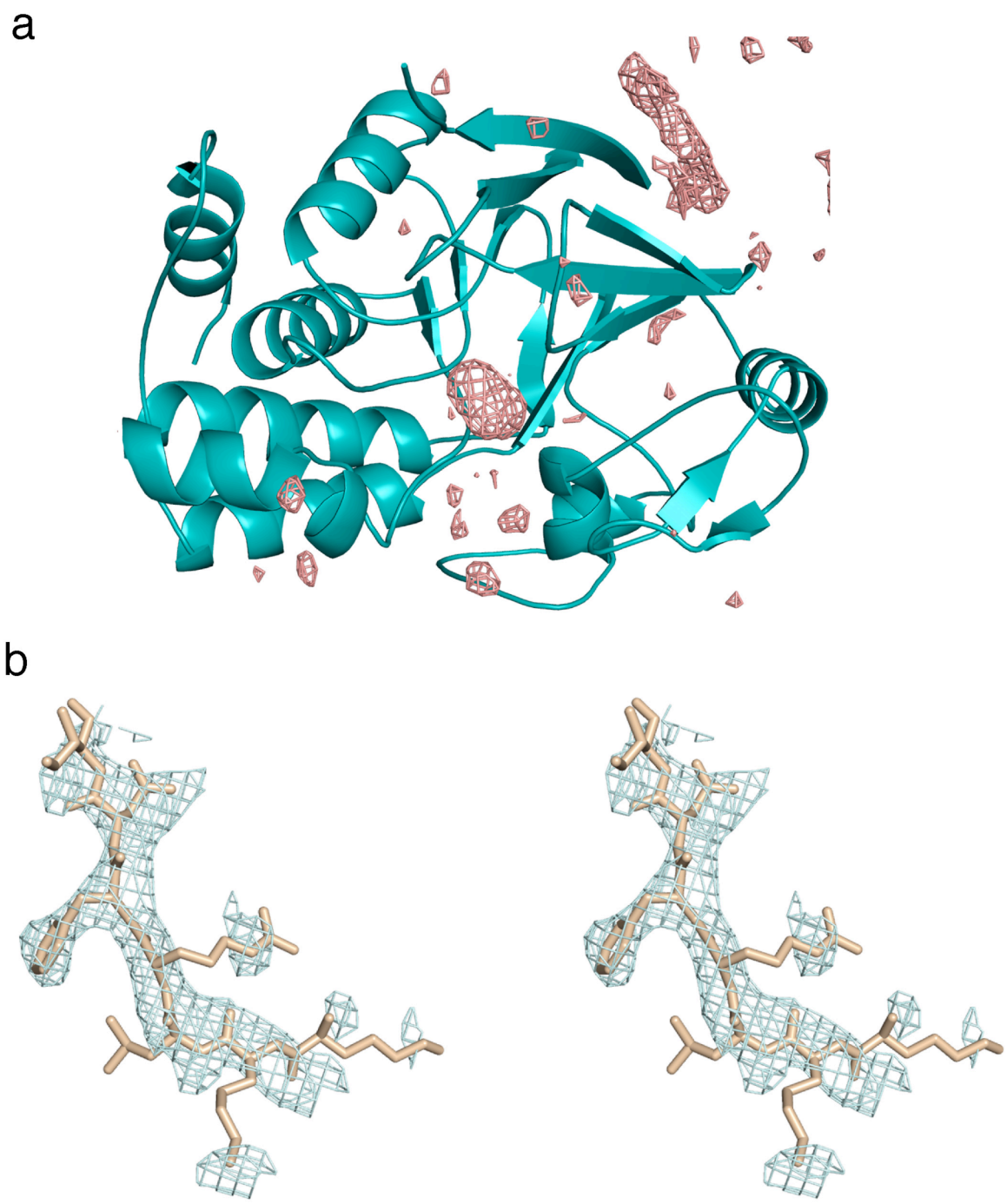

Supplementary Figure 3 Sample electron density maps. (a) Difference map (F_o-F_c; pink) calculated using the experimental structure factors (F_o) and structure factors calculated from the refined PP1c model (F_c) as fourier coefficients. The map is contoured at 3.5σ. The density peak in the center of the molecule is at the catalytic site

and likely corresponds to Mn^{2+} ions left out of the model at this stage of refinement. The significant density at the top right was assigned as the RbC peptide. The PP1c model is shown in cyan. (b) Stereo representation of the RbC peptide (residue 873-879) in the final model. A simulated-annealing omit (F_o-F_c) electron density map (cyan) is contoured at 2σ.

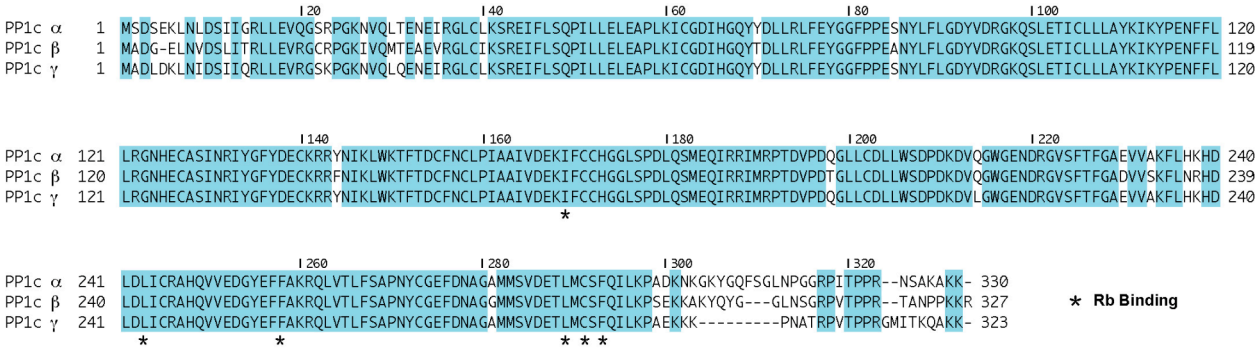

Supplementary Figure 4 Sequence alignment of human PP1c isoforms. The residues involved in Rb binding are conserved in all three paralogs.

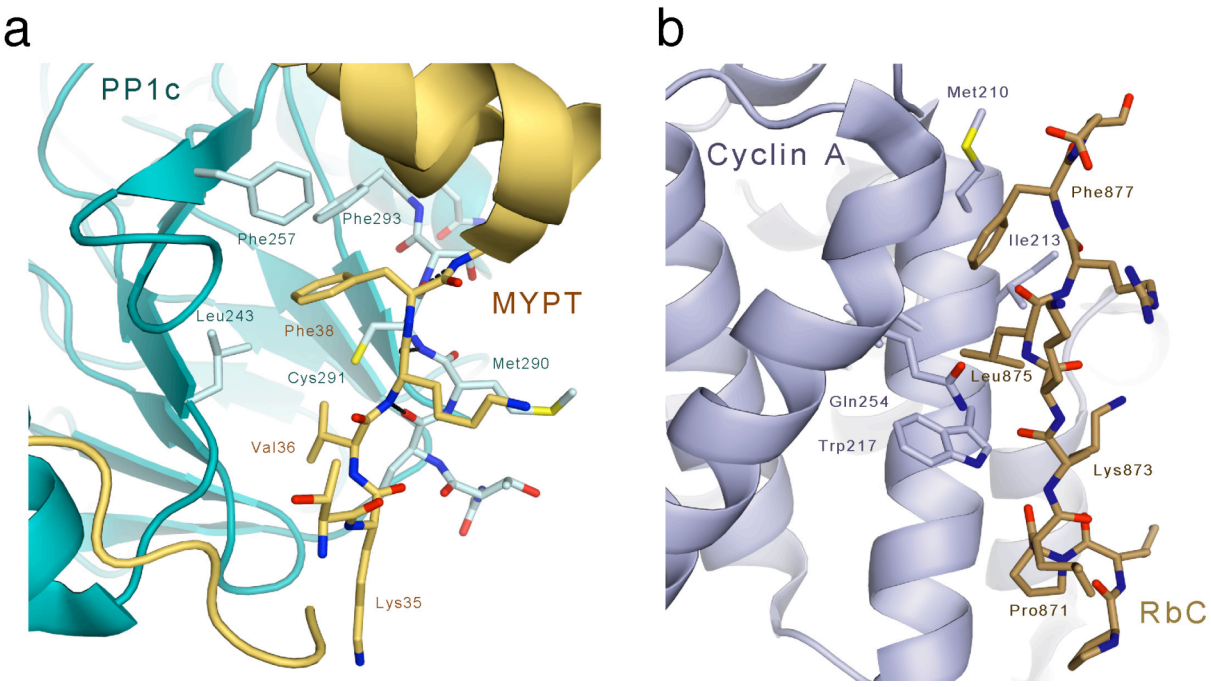

Supplementary Figure 5 Structural comparison of the RbC-PP1c docking interaction. (a) Structure of the myosin phosphate targeting (MYPT) subunit (yellow) bound to PP1c[20]. Comparison to the RbC$^{870\text{-}882}$-PP1c structure in Fig. 2 shows a similar mode of PP1c binding between Rb and the RVxF motif of PP1 regulatory subunits. (b) Structure of Rb$^{870\text{-}878}$-Cdk2-CycA complex[31]. Leu875 and Phe877 sidechains in Rb bind to a hydrophobic cleft in Cyclin A (violet).

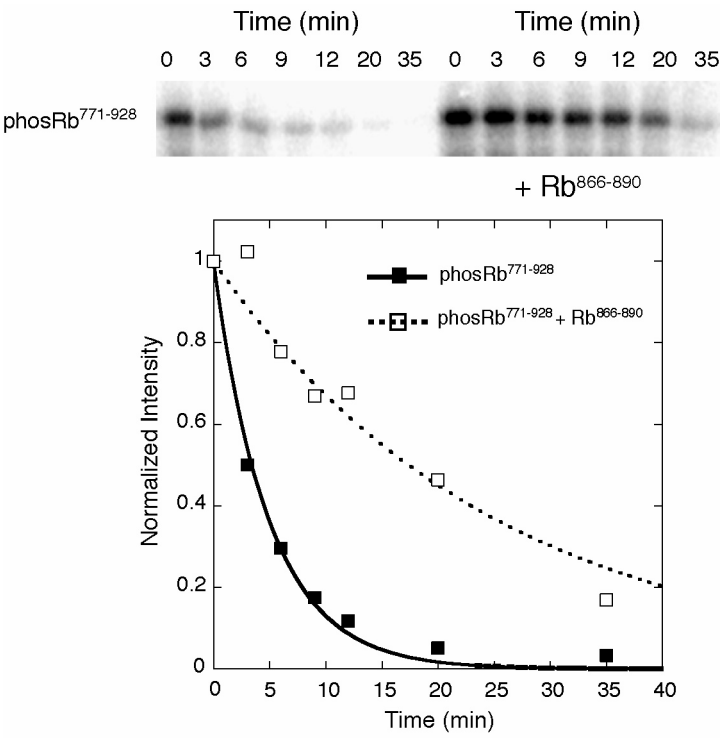

Supplementary Figure 6 A synthetic peptide containing 'KLRF' inhibits Rb-directed PP1 activity. Addition of excess synthetic $Rb^{866-890}$ peptide, which contains the PP1c 'KLRF' docking sequence, inhibits the phosphatase reaction with $phosRb^{771-928}$. Addition of a saturating quantity of $RbC^{866-890}$ peptide reduces the first-order rate constant for dephosphorylation of $phosRb^{771-928}$ from $k_{dephos} = 0.20 \pm 0.01$ min^{-1} (■) to $k_{dephos} = 0.040 \pm 0.004$ min^{-1} (□). The reduced value is comparable to the value for dephosphorylation of the substrate that lacks the docking site ($k_{dephos} = 0.027 \pm 0.002$ min^{-1}; Fig. 3c). Based on these data and mutagenesis data presented in Fig. 3, we conclude that the KLRF docking site on Rb is required for efficient recognition and dephosphorylation by PP1c.

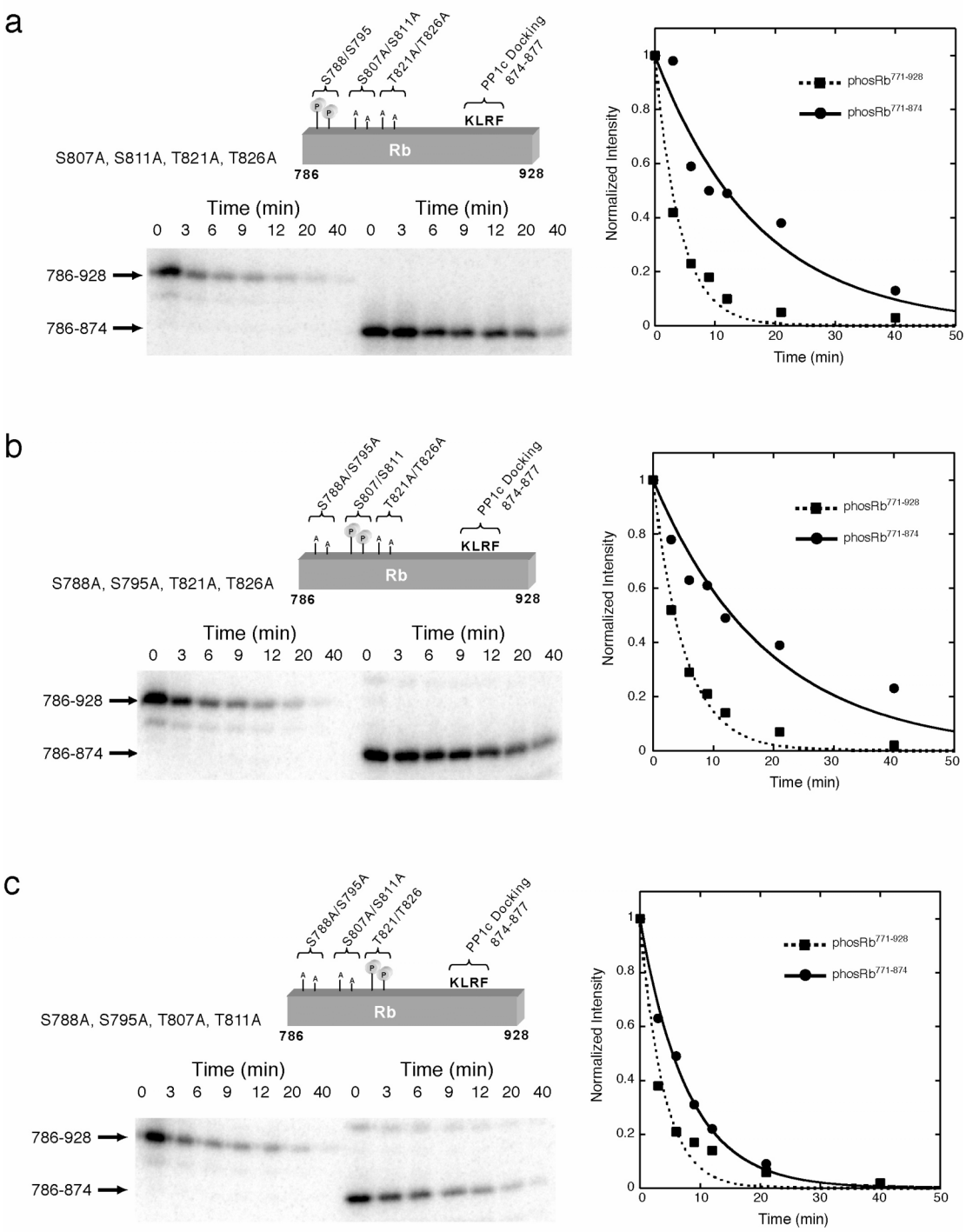

Supplementary Figure 7 Phosphatase assays on specific phosphoacceptor sites in RbC. Phosphatase assays were performed on fragments of RbC that were phosphorylated at only one pair of proximal phosphoacceptor sites. Specificity of phosphate incorporation

in the kinase reaction was achieved my mutating other phosphoacceptor sites to alanine. Assays were conducted as in Fig. 3 except that 2 μM of each phosphorylated and purified substrate was incubated with 15 nM enzyme. Each panel contains a schematic indicating the specific phosphoacceptor pair being dephosphorylated, a Phosphorimage of the quenched reaction aliquots, and the quantified band intensities as a function of time. For each phosphorylated pair, dephosphorylation rates are decreased by truncation of the KLRF docking motif. The fits are assuming first-order dephosphorylation kinetics. (a) S788/S795 dephosphorylation. phosRbC$^{786-928}$: k_{dephos} = 0.24 ± 0.02 min^{-1}; phosRbC$^{786-874}$: k_{dephos} = 0.058 ± 0.008 min^{-1}. (b) S807/S811 dephosphorylation. phosRbC$^{786-928}$: k_{dephos} = 0.19 ± 0.01 min^{-1}; phosRbC$^{786-874}$: k_{dephos} = 0.053 ± 0.006 min^{-1}. (c) T821/T826 dephosphorylation. phosRbC$^{786-928}$: k_{dephos} = 0.26 ± 0.03 min^{-1}; phosRbC$^{786-874}$: k_{dephos} = 0.128 ± 0.005 min^{-1}.

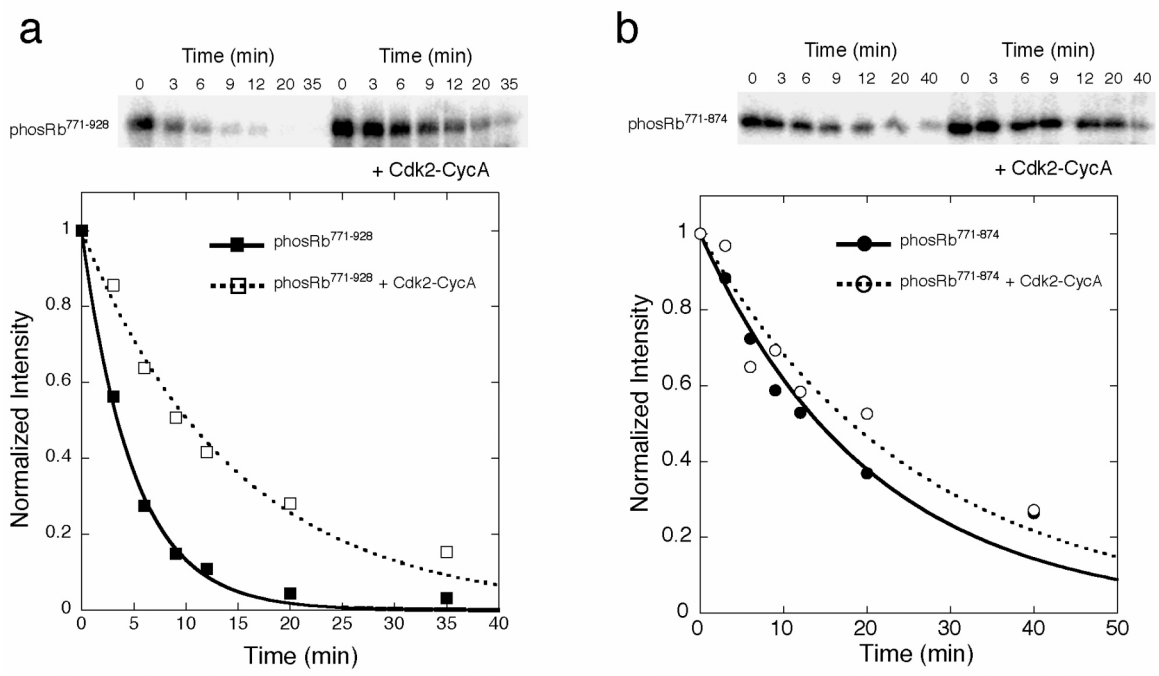

Supplementary Figure 8 Cdk2-CycA inhibits Rb-directed PP1c activity in a docking site dependent manner. In a reaction with PP1c and phosRbC$^{771\text{-}928}$ and without ATP, we characterized the effect of inactive Cdk2-CycA on the rate of RbC directed PP1c activity. (a) Addition of a saturating quantity of Cdk2-CycA inhibits dephosphorylation of phosRbC$^{771\text{-}928}$, reducing the first-order rate constant from k_{dephos} = 0.20 ± 0.01 min^{-1} to k_{dephos} = 0.068 ± 0.004 min^{-1}; this latter rate constant in the presence of kinase is similar to the rate constant for dephosphorylation of phosRbC$^{771\text{-}874}$. (b) Addition of Cdk2-CycA to the phosRbC$^{771\text{-}874}$ dephosphorylation reaction has little effect on the first order rate constant, changing it from k_{dephos} = 0.049 ± 0.004 min^{-1} to k_{dephos} = 0.038 ± 0.005 min^{-1}.

Supplementary Information/Methods

Crystal Structure Refinement

Initial crystals grown with full length PP1c diffracted to moderate resolution (~4 Å). We attempted to improve resolution by deleting residues 301-330 from PP1c, as these residues were not observed in previous PP1c structures and are presumed disordered[34,35]. Crystals of an $Rb^{870-882}$-$PP1c^{1-300}$ grew with the same morphology and unit cell parameters as the crystals using full-length PP1c but diffracted with improved resolution. $Rb^{870-882}$ binds to $PP1c^{1-300}$ with the same affinity as full length PP1c as determined by ITC (data not shown).

The highest quality diffraction data were collected from crystals of an $Rb^{870-882}$-$PP1c^{1-300}$ complex (see Methods and Table 1). Diffraction data were collected using Beamline 5.0.1 of the Advanced Light Source (Lawrence Berkeley National Laboratories). Data were indexed and scaled with Mosflm and SCALE-IT. The structure was determined with molecular replacement using PP1c alone as an initial model. Two molecules of PP1c are observable in the asymmetric unit, and an initial difference electron density map revealed two significant peaks near each of the two PP1c molecules (Supplementary Fig. 3a). One peak is near the enzyme active site and corresponds to known, bound Mn^{2+} ions. The other significant feature in the difference map shows clear density corresponding to seven residues of the $Rb^{870-882}$ peptide. Sidechain density in the center of the initial difference map peak could confidently be assigned to Phe877. Accordingly, the rest of the peptide was fit, and the model of the $Rb^{870-882}$-PP1c complex was further refined (Supplementary Fig. 3b).

The Rb peptide was built into the model with COOT, and the entire model further refined with Phenix using standard rigid body, simulated annealing, and temperature factor refinement routines. The similar structures of the two PP1c molecules in the asymmetric unit motivated the use of noncrystallographic symmetry during refinement. Electron density corresponding to RbC was observed near both PP1c molecules, however, it was significantly more interpretable in one of the two complexes, and only one RbC peptide was included in the model. We believe that the intensity difference in RbC electron density results from different occupancies or dynamics; the peptide built into the more interpretable density makes crystal-packing contacts that may stabilize it, whereas the other density in the other asymmetric unit is solvent exposed.

Calorimetry Binding Experiments with RbC Docking Site Mutants

We tested how mutation of the overlapping binding site affects the affinity of RbC for both PP1c and Cdk2-CycA. As seen in Fig. 1d, PP1c binds to $RbC^{866-928}$ with $K_d = 2.1 \pm 0.8$ μM. Mutation of F877 to alanine ($RbC^{866-928\_F877A}$) and L875 to arginine ($RbC^{866-928\_L875R}$) in this construct resulted in no detectable ITC signal (Supplementary Fig. 2), which is consistent with a lack of a significant association. Arginine was chosen because of its known intolerance at the V position in the 'RVxF' motif of PP1c regulatory subunits. The observed lack of binding corroborates our structural data showing that Leu875 and Phe877 make critical contacts to the PP1c β-sandwich subdomain.

We next tested binding of $RbC^{866-928}$ to Cdk2-CycA and measured a dissociation constant of $K_d = 6.3 \pm 0.7$ μM (Supplementary Fig. 2), which is similar to that previously measured for a shorter RbC peptide[31]. ITC experiments titrating $RbC^{866-928\_F877A}$ and

$RbC^{866\text{-}928\_L875R}$ into Cdk2-CycA resulted in no detectable signal, indicating that F877 and L875 are also required for the RbC-Cdk2-CycA association.